

BARBARA KLEMCZAK, AGNIESZKA KNOPPIK-WRÓBEL*

NUMERICAL MODEL FOR ANALYSIS OF EARLY-AGE THERMAL–MOISTURE EFFECTS IN AN RC WALL

MODEL NUMERYCZNY DO ANALIZY WCZESNYCH WPLYWÓW TERMICZNO-WILGOTNOŚCIOWYCH W ŚCIANIE ŻELBETOWEJ

Abstract

The paper presents the original numerical model for simulation of thermal, moisture and mechanical effects in concrete structures with an example of application. The influence of different curing conditions on the temperature and moisture distribution in RC wall was investigated. The stress state and the damage intensity factor were determined and the areas of possible cracking were selected as well.

Keywords: early-age concrete, FEM analysis, thermal–shrinkage stresses, RC wall

Streszczenie

W artykule przedstawiono autorski model numeryczny do symulacji zjawisk termicznych, wilgotnościowych i mechanicznych w konstrukcjach betonowych wraz z przykładem jego zastosowania. Zbadano wpływ warunków betonowania i pielęgnacji na rozkład temperatur i wilgotności w ścianie żelbetowej. Wyznaczono stan naprężenia oraz wyężenia, określając również możliwe obszary zarysowania.

Słowa kluczowe: młody beton, analiza MES, naprężenia termiczno-skurczowe, ściana żelbetowa

* DSc. Eng. Barbara Klemczak, MSc. Eng. Agnieszka Knoppik-Wróbel, Department of Structural Engineering, Faculty of Civil Engineering, Silesian University of Technology.

1. Introduction

In the phase of concrete structures erection, the loads originating from the material of which a structure is made play a significant role. These loads, caused by temperature and humidity changes of early-age concrete, are defined as indirect interactions. Temperature changes in a concrete structure are related to the exothermic nature of cement hydration. The concrete temperature increases as a result of heat released in this process. The cooling of surface layers of the structure and a relatively low value of concrete thermal conductivity result in temperature differences between the surface layers and the interior of the structure. Concrete curing is also accompanied by a migration of moisture. It is caused by the process of cement hydration and moisture exchange within the environment in conditions of variable temperatures. Thus the movement of moisture may result from moisture diffusion, i.e. from the existence of moisture concentration gradients, and from the thermal diffusion, i.e. due to the existence of temperature gradients.

The originating non-linear and non-stationary coupled thermal–moisture fields generate self-induced stresses in the structure (related to internal constraints of the structure, resulting from inhomogeneous distribution of thermal–moisture fields) and restraint stresses (related to limitation of structure deformations freedom). These stresses can reach a significant level and as a consequence, cracking may occur. Two kinds of cracking in early-age concrete can be distinguished. In massive members, such as thick foundation blocks, a significant temperature generated during the hydration process is generally different in each point of the structure. The tensile stresses are induced by differences between the interior and surface temperatures of the block. Although the interaction with subsoil limits the possibility of deformations, the self-induced stresses are predominant in such structures. In medium-thick structures such as walls, the thermal and shrinkage deformations are usually prevented by a restraint, e.g. if a wall is cast against an old set concrete. The cracking develops mainly due to restraint stresses generated by shrinkage and thermal effects.

2. Modeling strategy

Early-age concrete is undoubtedly one of the most difficult structural materials for modeling. The difficulties arise from a complex concrete structure which is additionally subjected to transformations as a result of cement hydration. Initially, it is a mixture of liquids and solids of varying diameters and shapes. Such a medium is characterized with strong viscous and plastic properties. With progressing cement hydration, concrete becomes a solid, with elastic, viscous and plastic characteristics, where the mutual proportions of these features depend on the concrete hardening advancement. Taking into account the concrete structure and its changes during hardening, two possibilities to model early-age concrete appear.

The first approach is related to structural models, in which a precise analysis of the physical phenomena and the material's internal structure influence on these phenomena is made. Appropriate constitutive equations describing the migration of heat, moisture and stress state are derived for the solid, liquid and gaseous phase of the medium and then averaged for a multi-phase medium. The second approach is related to phenomenological models where concrete is treated as a continuous medium. A detailed analysis of physical processes related

to phase transitions and chemical processes occurring in hardening concrete is neglected in these models and a macroscopic description of the thermal–moisture–mechanical phenomena is used. It should be mentioned that the phenomenological models are applied more often for the analysis of the discussed phenomena [1–6] but there are also some proposals of the structural models [7–9].

The next issue in modeling of the early-age concrete is an approach to coupling of temperature, moisture and stresses. In this field, it is possible to assume a full coupling of thermal–moisture–mechanical fields and to separate thermal–moisture and mechanical fields. The first approach takes into account the influence of mechanical field changes on changes of concrete temperature and humidity. In the second approach, the influence of the mechanical field on thermal diffusion processes is neglected. In such a model, the thermal–moisture fields are determined first. The stress state is determined assuming that the thermal–shrinkage strains, defined based on temperature and humidity changes, have a distortional nature. In turn, in the area of thermal–moisture fields modelling, it is possible to assume a full coupling of thermal and humidity fields to neglect the influence of humidity changes on temperature changes (partial coupling of equations) and also to assume uncoupled equations. At this point, it is important to mention that in many models proposed for the description of thermal and moisture fields, the equations are formulated independently, neglecting their coupling [10–11].

It is also necessary to assume appropriate material model of early-age concrete as the basis to define the stress state and the damage intensity of the structure. The material model should consider variability of concrete mechanical properties related to its aging as well as viscous effects. Viscous effects should not be neglected in the model, both due to a long-term nature of thermal–shrinkage loads and properties of early-age concrete, which shows features of this type much stronger than in the mature concrete. Now, to evaluate thermal–shrinkage stresses, a viscoelastic model is most often used [1–6] but attempts are also made to use more advanced models: viscoelasto–plastic [12], elasto–viscoplastic [13] or viscoelasto–viscoplastic [14] models.

3. Numerical model

The presented numerical model can be classified as a phenomenological model. The influence of the mechanical fields on the temperature and moisture fields was neglected, but the thermal–moisture fields were modeled using the coupled equation of the thermodiffusion. Therefore, the complex analysis of a structure consists of three steps. The first step is related to the determination of temperature and moisture development, in the second one, thermal–shrinkage strains are calculated and these results are used as an input for computation of stress in the last step. For the purpose of determination of the stress state in the early-age concrete structures, the viscoelasto–viscoplastic model with a consistent conception was proposed. The proposed model is an extension of the earlier proposed viscoelasto–plastic model. With respect to the engineering application of the theoretical models, the computer programs were also developed. Some details of the model are given below and a full description of the model and computer programs: TEMWIL, MAFEM_V EVP and MAFEM3D, is contained in [15].

3.1. Thermal and moisture analysis

The coupled temperature and moisture fields in early-age concrete can be described by the following equations [15–16]:

$$\dot{T} = \text{div}(\alpha_{TT} \text{grad } T + \alpha_{TW} \text{grad } c) + \frac{1}{c_b \rho} q_v \quad (1)$$

$$\dot{c} = \text{div}(\alpha_{WW} \text{grad } c + \alpha_{WT} \text{grad } T) - K q_v \quad (2)$$

where:

- T – temperature [K],
- c – moisture concentration [kg/kg],
- $\dot{T} = \frac{\partial T}{\partial t}$ – time derivative of temperature,
- $\dot{c} = \frac{\partial c}{\partial t}$ – time derivative of moisture concentration,
- α_{TT} – coefficient of thermal diffusion [m^2/s],
- α_{WW} – coefficient of moisture diffusion [m^2/s],
- α_{TW} – coefficient representing the influence of moisture concentration on heat transfer [$\text{m}^2\text{K}/\text{s}$],
- α_{WT} – thermal coefficient of moisture diffusion [$\text{m}^2/(\text{sK})$],
- c_b – specific heat [$\text{kJ}/(\text{kgK})$],
- ρ – density of concrete [kg/m^3],
- K – coefficient of water–cement proportionality, which describes the amount of water bounded by cement during the hydration process with the rate of heat generated by cement hydration per unit volume of concrete [m^3/J],
- q_v – rate of heat generated by cement hydration per unit volume of concrete [W/m^3].

Initial and boundary conditions may be expressed as follows:

$$T(x_i, t = 0) = T_p(x_i, 0) \quad (3)$$

$$c(x_i, t = 0) = c_p(x_i, 0) \quad (4)$$

$$\mathbf{n}^T (\alpha_{TT} \text{grad } T + \alpha_{TW} \text{grad } c) + \tilde{q} = 0 \quad (5)$$

$$\mathbf{n}^T (\alpha_{WW} \text{grad } c + \alpha_{WT} \text{grad } T) + \tilde{\eta} = 0 \quad (6)$$

where $x_i \in (V \cup \partial V)$, $i = x, y, z$, T_p , c_p are the initial distribution of temperature and the initial concentration of moisture, respectively, $\mathbf{n} = [n_x, n_y, n_z]^T$ is a vector normal to the boundary surface ∂V .

The heat flux \tilde{q} depends on the temperature of the boundary surface $\hat{T}(x_i, t)$ and the outer temperature $T_z(t)$. Similarly, the moisture flux $\tilde{\eta}$ depends on the moisture content at the boundary surface $\hat{c}(x_i, t)$ and on the moisture content in the surrounding air. Hence, it can be written:

$$\tilde{q} = \frac{\alpha_p}{c_b \rho} [\hat{T}(x_i, t) - T_z(t)] \quad (7)$$

$$\tilde{\eta} = \beta_p [\hat{c}(x_i, t) - c_z(t)] \quad (8)$$

where α_p denotes the thermal transfer coefficient, W/(m²K), β_p is the moisture transfer coefficient, m/s and c_z can be calculated from the formula:

$$c_z = \frac{W_z \rho_w}{\rho} \quad (9)$$

with $W_z = 0.0005\varphi$, m³/m³, and $\rho_w = m_w / V_w$, where:

φ – relative humidity [%],

m_w – mass of water in concrete [kg],

V_w – volume of water in concrete [m³].

Taking into account the amount of cement c_c in 1 m³ of concrete mix, the rate of heat generated per unit volume of concrete can be determined as:

$$q_v(T, t) = c_c q(T, t) \quad (10)$$

The rate of heat generated per unit volume of cement can be written as follows:

$$q(T, t) = \frac{\partial Q(T, t)}{\partial t} \quad (11)$$

In the presented model, heat of hydration was described by the equation:

$$Q(T, t) = Q_\infty e^{-at_e^{-0.5}} \quad (12)$$

where a is the coefficient connected with the type of cement given by the function $a = a_1 t_e^{a_2}$ (a_1 and a_2 depend on the type of cement) and t_e is the equivalent age of concrete that is given by the equation:

$$t_e = \int_0^t e^{-\frac{E_K}{R} \left(\frac{1}{T} - \frac{1}{T_0} \right)} dt \quad (13)$$

3.2. Thermal–shrinkage strains

Imposed thermal–shrinkage strains ε^n are treated as volumetric strains:

$$d\boldsymbol{\varepsilon}^n = \begin{bmatrix} d\varepsilon_x^n & d\varepsilon_y^n & d\varepsilon_z^n & 0 & 0 & 0 \end{bmatrix} \quad (14)$$

and calculated based on predetermined temperature and humidity according to the equation:

$$d\varepsilon_x^n = d\varepsilon_y^n = d\varepsilon_z^n = \alpha_T dT + \alpha_W dW \quad (15)$$

where:

α_T – the coefficient of thermal deformability,

α_W – the coefficient of moisture deformability.

Equation 15 has a simplified character, because it assumes a linear relationship between temperature and moisture change in hardening concrete and strains. Although some authors suggest a non-linear relationship, especially in description of shrinkage strains based on moisture change, the relationship in Equation 15 is most frequently used in modelling of the phenomena being considered. The relation between mass concentration c (kg/kg) and volumetric moisture W (m³/m³) can be expressed analogically to equation (9).

3.3. Stress analysis

In the model, the viscoelastic and viscoelasto–viscoplastic areas were distinguished. These two areas are separated by the initial location of the yield surface, the formula of which is defined by the boundary surface multiplied by the coefficient less than one. The coefficient can be classified as the viscoelasticity limit. Its value depends on the concrete strength in uniaxial compression, as in the equation:

$$e_{\text{lim}} = 1 - e^{-0.02f_c(t_e)} \quad (17)$$

The following constitutive equation was assumed in the viscoelastic area:

$$\dot{\boldsymbol{\sigma}} = \mathbf{D}^{\text{ve}} (\dot{\boldsymbol{\varepsilon}} - \dot{\boldsymbol{\varepsilon}}^n - \dot{\boldsymbol{\varepsilon}}^c) \quad (18)$$

where:

$$\dot{\boldsymbol{\sigma}} = \frac{d\boldsymbol{\sigma}}{dt}, \quad \dot{\boldsymbol{\varepsilon}} = \frac{d\boldsymbol{\varepsilon}}{dt}, \quad \dot{\boldsymbol{\varepsilon}}^n = \frac{d\boldsymbol{\varepsilon}^n}{dt}, \quad \dot{\boldsymbol{\varepsilon}}^c = \frac{d\boldsymbol{\varepsilon}^c}{dt} \quad (19)$$

Viscoelasticity matrix $\mathbf{D}^{\text{ve}}(t_{i+1})$ is given by the formula:

$$\mathbf{D}^{\text{ve}}(t_{i+1}) = \frac{\mathbf{D}^e(t_{i+1})}{1 + 0.5E(t_{i+1}) \left[\frac{1}{E(t_i)} - \frac{1}{E(t_{i+1})} + H(t_{i+1}, t_i) \right]} \quad (20)$$

and additional denotations $\Delta \boldsymbol{\varepsilon}^c(t_{i+1})$ and $H(t_{i+1}, t_i)$ are given by the formulas:

$$\Delta \boldsymbol{\varepsilon}^c(t_{i+1}) = \mathbf{D}^{-1} \left[\int_0^{t_i} -\frac{\partial C(t_{i+1}, \tau)}{\partial \tau} \boldsymbol{\sigma}(\tau) d\tau + \boldsymbol{\sigma}(t_i) \int_{t_i}^{t_{i+1}} -\frac{\partial C(t_{i+1}, \tau)}{\partial \tau} d\tau - \int_0^{t_i} -\frac{\partial C(t_i, \tau)}{\partial \tau} \boldsymbol{\sigma}(\tau) d\tau \right] \quad (21)$$

$$H(t_{i+1}, t_i) = \int_{t_i}^{t_{i+1}} -\frac{\partial C(t_{i+1}, \tau)}{\partial \tau} d\tau \quad (22)$$

A creep function $C(t, \tau)$ and a function describing the modulus of elasticity variation during concrete curing $E(t)$ were assumed according to functions suggested by CEB FIP MC90 [17].

In the viscoelasto–viscoplastic area, the constitutive equation has a form:

$$\dot{\boldsymbol{\sigma}} = \mathbf{D}^{ve} (\dot{\boldsymbol{\varepsilon}} - \dot{\boldsymbol{\varepsilon}}^n - \dot{\boldsymbol{\varepsilon}}^c - \dot{\boldsymbol{\varepsilon}}^{vp}) \quad (23)$$

where:

$$\dot{\boldsymbol{\varepsilon}}^{vp} = \dot{\lambda} \frac{\partial f}{\partial \boldsymbol{\sigma}} \quad (24)$$

In the consistent concept of the viscoplastic strains description, both the yield surface f and the failure surface F are rate-dependent surfaces:

$$f(\boldsymbol{\sigma}, \boldsymbol{\kappa}, \dot{\boldsymbol{\kappa}}) = 0 \quad (25)$$

$$F(\boldsymbol{\sigma}, \boldsymbol{\kappa}, \dot{\boldsymbol{\kappa}}) = 0 \quad (26)$$

The failure surface can be described as a modified 3-parameter Willam–Warnke failure criterion [15, 16, 18]. The failure criterion involves all stress invariants in the form of non-dimensional values of the octahedral stress $s_m = \sigma_m / f_c(t_e)$, $t_0 = \tau_{okl} / f_c(t_e)$ and the angle of similarity θ . The failure surface for young concrete was assumed as a fixed surface in the proposed coordinate system. The meridians are straight lines and in the low-compression and tension regime, the caps described as the second-order parabolas were introduced. In the deviatoric plane, the failure surface in both models has a noncircular cross-section, described according to the Willam–Warnke conception as a part of an elliptic curve (Fig. 1).

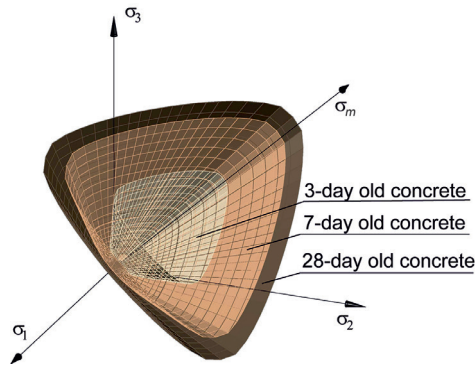


Fig. 1. Development of the failure surface of young concrete in the maturing process

A smeared crack image was assumed in the model. The possibility of crack occurrence is defined based on the location of the point representing a stress state with respect to the failure surface. This location can be described by the formula:

$$s_l = \frac{\tau_{okt}}{\tau_{okt}^f} \tag{27}$$

where:

s_l – referred to as the damage intensity factor.

The damage intensity factor equal to 1 is equivalent to the stress reaching the failure surface and signifies failure of the element. Character of this failure depends on the location where the failure surface is reached [15–16]. In the further presented examples, reaching of the failure surface always occurred within the range of the hydrostatic tensile stresses which is equivalent to formation of the crack in the plane perpendicular to the direction of the maximum principal stress.

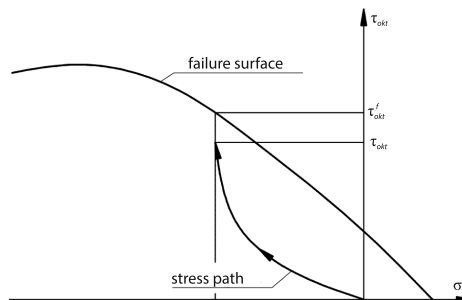


Fig. 2. Axi-torric section of failure surface

3.4. Reinforcement

Reinforcement is modelled as bar elements connected with concrete elements in the nodes. Bond forces between reinforcement and adjoining concrete are not considered, so the assumed model is simplified. Elastic–perfectly-plastic material model with Huber–von Mises–Hencky failure surface is assumed for reinforcement.

3.5. Validation of the model

Validation of the numerical results with experimentally-obtained data is necessary to confirm reliability of the theoretical model. Because the proposed model includes two issues connected with determination of thermal–moisture fields and stress and strain states, validation of the model should be two-phase. It should be noted that this is an untypical task in which firstly the loads to which the structure is subjected (thermal–moisture fields) are validated, and then the effects of these loads – stress state – is validated. This results from a specific nature of massive concrete structures where the material of the structure itself is the source of the load.

Validation of the model is presented in [15]. In the validation of thermal–moisture fields, the authors' own experimental results were used. In the case of stress state, because of the assumed complex material model, validation was initially performed with simple numerical tests, which allowed for qualitative confirmation of the proposed material model correctness. Firstly, creep test simulation in heavily stressed conditions was performed. Then, the results of numerical simulations of simple stress states in concrete samples were presented, i.e. uniaxially compressed and tensiled samples and cylindrical samples in split test. In the second phase, the thermal–shrinkage stresses were analysed. The results of the authors' own, as well as other experiments were used.

4. Analysis of RC wall

4.1. Input data

The analysed wall was assumed to have 20 m of length, 4 m of height and 80 cm of thickness, supported on a 4 m wide and 70 cm deep strip foundation of the same length. The wall and the foundation were assumed to be reinforced with a near-surface reinforcing net of $\varnothing 16$ bars. The wall was reinforced at both surfaces with horizontal spacing of 20 cm and vertical spacing of 15 cm. The foundation was reinforced with a 20 cm \times 20 cm mesh at the top and bottom surface.

Due to the fact that the wall has two axes of symmetry, the model for finite element analysis was created for $\frac{1}{4}$ of the wall. A uniform mesh was prepared and densified at the free edges of the wall and within the contact surface between the wall and the foundation. The final geometry of the wall with a mesh of finite elements is presented in Fig. 3.

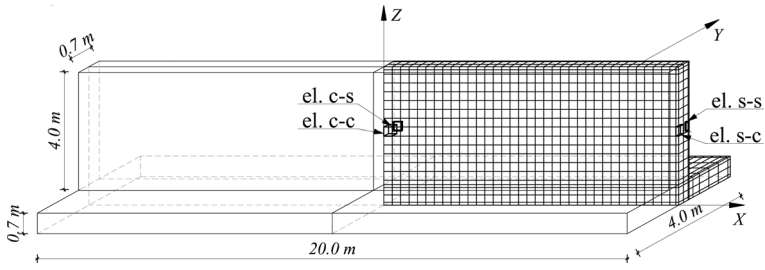


Fig. 3. Dimensions of the wall with finite element mesh

Mechanical properties of mature concrete were taken as follows: the compressive strength $f_{cm} = 35$ MPa, the tensile strength $f_{ctm} = 3$ MPa and the modulus of elasticity $E_{cm} = 32$ GPa, and steel class RB400 were assumed for both the wall and the foundation. The foundation was erected earlier and had hardened, so the material properties were assumed as for 28-day concrete. For the wall, development of material properties was assumed according to CEB-FIP MC90. Detailed material properties, environmental and technological conditions were taken as:

- cement type CEM I 42.5R, 375 kg/m³,
- concreting proceeded in summer – ambient temperature $T_z = 25^\circ\text{C}$,
- initial temperature of fresh concrete mixture $T_p = T_z = 25^\circ\text{C}$,
- wooden formwork of 1.8cm plywood; no insulation,
- protection of top surface with foil,
- formwork removed in 3 days (72 h) after concrete casting.

The values of parameters taken in numerical analysis are presented in Table 1.

Table 1

Parameters assumed for numerical analysis

| Thermal fields | | Moisture fields | |
|------------------------------------|--|------------------------------------|--|
| Λ [W/(mK)] | 2.56 | q_v [W/m ³] | acc. to eq. (10)* |
| c_b [kJ/(kgK)] | 0.82 | | |
| ρ [kg/m ³] | 2413 | K [m ³ /J] | $0.3 \cdot 10^{-9}$ |
| α_p [m ² /s] | $12.94 \cdot 10^{-7}$ | α_{ww} [m ² /s] | $0.6 \cdot 10^{-9}$ |
| α_{TW} [m ² K/s] | $9.375 \cdot 10^{-5}$ | α_{wT} [m ² /sK] | $2 \cdot 10^{-11}$ |
| α_p [W/(m ² K)] | 15.00 no covering 13.78 foil 5.58 formwork | β_p [m/s] | $2.78 \cdot 10^{-8}$ no covering $0.10 \cdot 10^{-8}$ foil $0.18 \cdot 10^{-8}$ formwork |

* data from tests for cement CEM I 42.5R: $Q_\infty = 508$ kJ/kg, $a_1 = 513.62$ and $a_2 = -0.17$

The foundation was assumed to have cooled down by the moment of wall casting, thus the initial temperature of the foundation concrete was taken as equal to the ambient temperature T_z . The parameters connected with temperature and moisture migration in the wall after formwork removal were assumed as for a free, unprotected surface.

4.2. Thermal and moisture analysis

The thermal–moisture effects were analyzed in time steps for the first 20 days (480 h) after casting of fresh concrete. Calculations were performed with TEMWIL program.

Fig. 4 shows the map of temperature distribution while Fig. 5 shows the map of moisture content distribution in the wall after 26 hours, when the maximum values of temperature were observed. It can be noticed that the concentration of high temperatures occurred in the central part of the wall while the edges were cooler because of the heat dissipation. Accompanying heating of the foundation was observed. It should be emphasised that there was little temperature difference at the thickness of the wall (not more than $\sim 6^\circ\text{C}$). Water content in the whole body of the wall was on a similar level; some moisture concentrated near the surfaces where the wall was protected with the formwork/foil.

A change of temperature and moisture content in time was examined for four finite elements to represent the behaviour of the interior and the surface of the wall in the central part and at the edge of the structure (the elements are marked in Fig. 3). The results are collectively presented in Fig. 6–7 for temperature and moisture content, respectively.

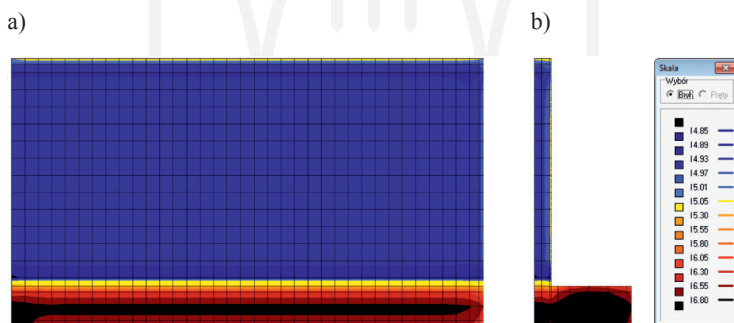


Fig. 4. Temperature distribution [$^\circ\text{C}$] after 26 hours: a) $XZ = 0$, b) $YZ = 0$

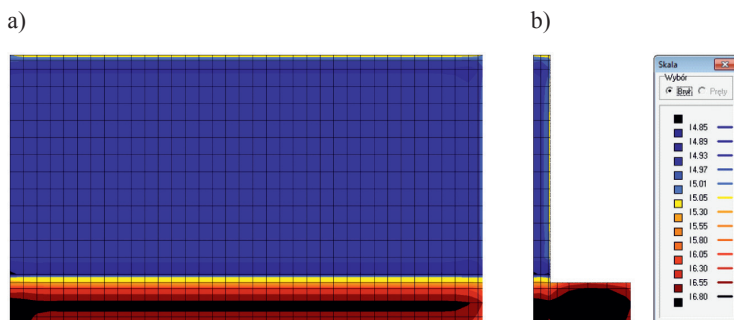


Fig. 5. Moisture content distribution [$\times 100, \text{m}^3/\text{m}^3$] after 26 hours: a) $XZ = 0$, b) $YZ = 0$

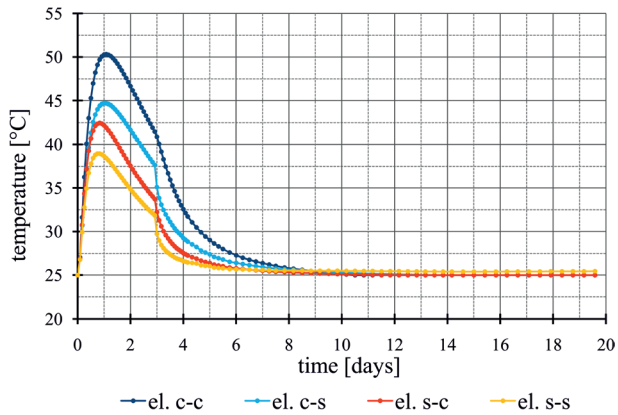


Fig. 6. Temperature evolution in time

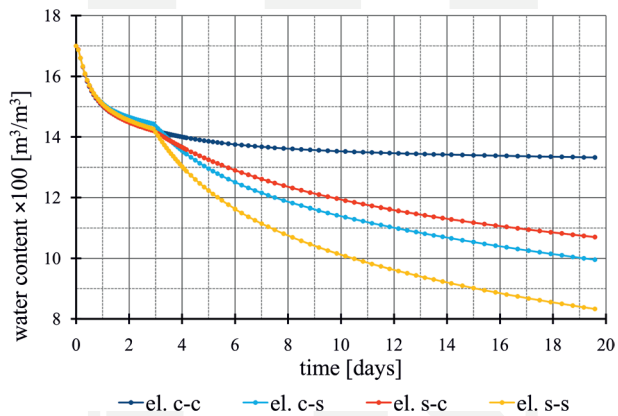


Fig. 7. Moisture loss in time

The greatest temperatures were reached in the central part of the wall, with maximum values obtained in the interior (el. c-c, 50.3°C) and bit smaller on the surface (el. c-s, 44.7°C). The lowest values were observed near the edge of the wall, with greater values inside the wall (el. s-c, 42.5°C) and smaller values near the surface (el. s-s, 38.9°C). The moment of formwork removal was visible, especially on the surface.

A similar pattern was also observed in the moisture migration diagram. The effect of the formwork removal was very visible: there was hardly any difference in the migration rate for different areas of the wall while the element was in the formwork, but the alteration was observed after the formwork was removed. As was expected, the rate of the drying process was decelerating as the accessibility to the surface decreased, being the fastest in the parts of the wall near two free surfaces (el. s-s), medium near one surface (el. s-c and c-s), and the slowest in the interior of the wall (el. c-c).

4.3. Stress analysis

Determination of the thermal–moisture fields allowed for the indication of the stress state and the level of damage intensity within the wall. Calculations were proceeded with MAFEM_V EVP program. The results were analysed with use of MAFEM3D interface. Figure 8 shows the change of σ_x stress in time.

Two distinct phases in the behaviour of the wall during concrete curing can be distinguished. The first phase was caused by thermal expansion of the wall due to increase of temperature. Because of the bond between the (cool) foundation and the (hot) wall, compressive stresses were induced in almost the whole wall. A map of stresses at expansion after 16 hours is presented in Fig. 9a. Deformation of the structure is presented in 500:1 scale with respect to dimensions of the structure. The second phase was connected with cooling of the concrete accompanied with extensive drying shrinkage occurring after formwork removal. This led to contraction of the wall and tensile stresses appearing in the wall. Fig. 9b presents a map of stresses after 6 days. The concrete of the wall is vulnerable to cracking if tensile stresses reach the level exceeding the tensile strength of concrete. A sudden drop of stress in the surface element in the diagram in Fig. 8 signifies that tensile strength was reached and a crack occurred in the element.

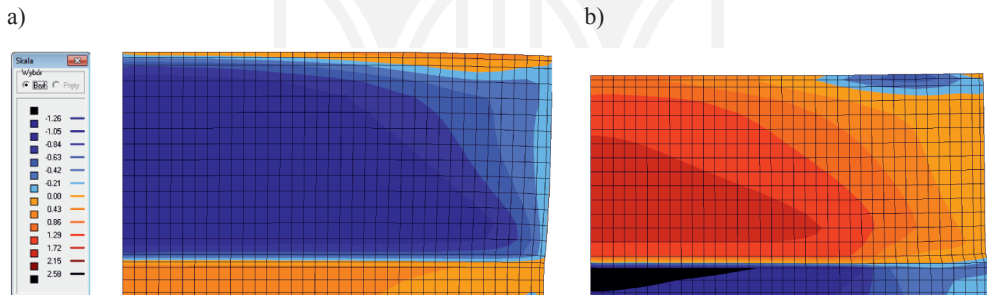


Fig. 9. σ_x stress distribution in $XZ = 0$ cross-section: a) heating phase, b) cooling phase

4.4. Parametric study of thermal–shrinkage cracking

The presented numerical model allows for a multi-parameter investigation of thermal–moisture effects in the early-age concrete. The influence of the factors connected with the geometry of the wall, environmental conditions as well as conditions of concreting and curing of concrete on the resultant thermal–shrinkage cracking can be analysed.

This paper presents the results of the investigation into the influence of the conditions of concrete casting and curing on cracking. The implemented smeared model of cracks means that cracking is not represented as single cracks but by means of the damage intensity factor diagrams, so the comparison of the results of the numerical simulation is based on the damage intensity maps. It was stated that in all the analysed cases, the failure surface was reached within the range of hydrostatic tensile stresses, thus each time the ultimate damage intensity factor was equal to 1 in the finite element, it was equivalent to formation of the crack within this element. Hence, the black areas in the damage intensity factor diagram represent the possible location of the cracks. The scale for damage intensity applies to all the maps.

Fig. 10 shows the damage intensity maps for the basic case after 19 days. A typical cracking pattern can be observed: vertical cracks occur within the wall with the biggest cracks concentrating in the midspan and decreasing towards the free edge of the wall. It should be noticed that due to the early formwork removal, the surface of the wall is more prone to rapid cooling and drying, hence cracking would be observed at the surface first and would be of greater magnitude in the near-surface areas.

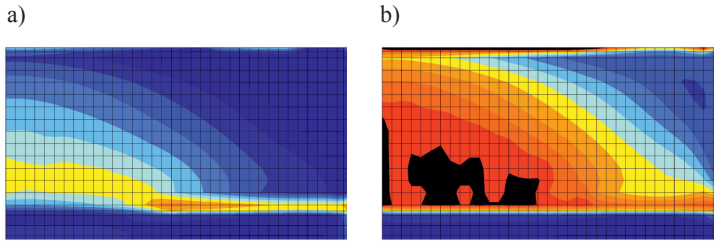


Fig. 10. Damage intensity of the wall in 19 days: a) $XZ = 0$, b) $XZ = 0.4$ m

4.4.1. Influence of ambient temperature and temperature difference

In the basic case, it was assumed that the concrete casting of the wall was proceeded during summer with no pre-cooling of the concrete mix. The second analysed example was a case of concreting in spring with the assumed ambient temperature of 15°C . The map of the damage intensity for that case after 19 days is presented in Fig. 11. It can be noticed that the character of damage intensity development is similar but the intensity is a bit lower.

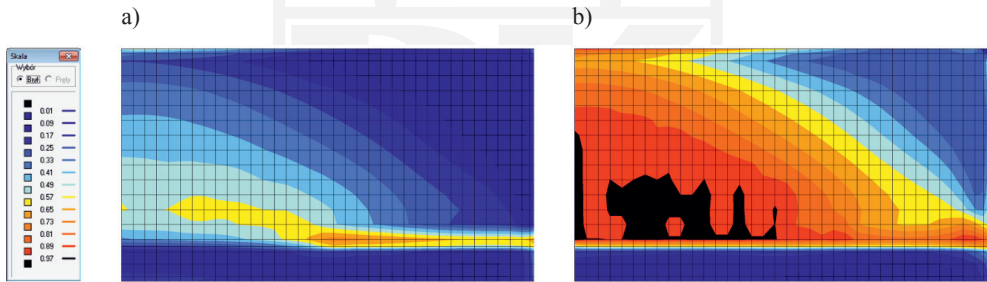


Fig. 11. Damage intensity of the wall in 19 days ($T_p = T_z = 15^{\circ}\text{C}$): a) $XZ = 0$, b) $XZ = 0.4$ m

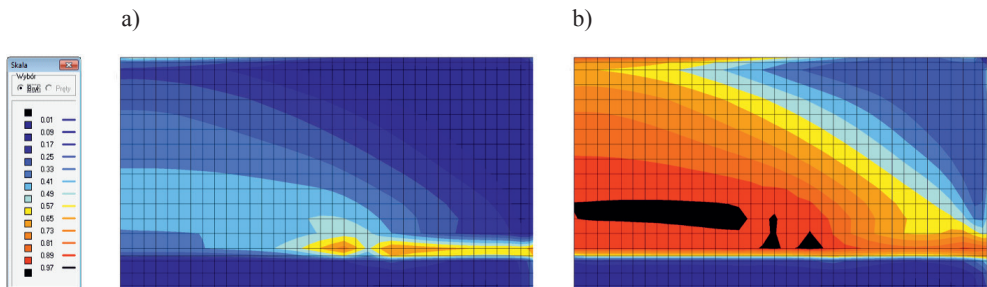


Fig. 12. Damage intensity of the wall in 19 days ($T_z = 25^{\circ}\text{C}$, $T_p = 20^{\circ}\text{C}$): a) $XZ = 0$, b) $XZ = 0.4$ m

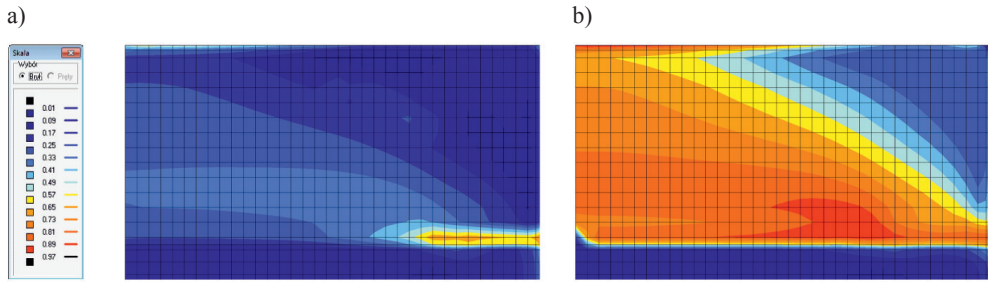


Fig. 13. Damage intensity of the wall in 19 days ($T_z = 25^\circ\text{C}$, $T_p = 15^\circ\text{C}$): a) $XZ = 0$, b) $XZ = 0.4$ m

In two other cases, the concrete casting was assumed to be proceeded in summer ($T_z = 25^\circ\text{C}$) but with the concrete mix cooled by 5 and 10°C ($T_p = 20$ and 15°C). The maximum observed temperature in the wall was reduced to 45.9 and 41.8°C , respectively. Fig. 12–13 present the maps of damage intensity after 20 days. A limitation of cracking was achieved – when initial cooling by 10°C was applied, cracking risk was completely eliminated.

The comparison was made between the basic case and the analysed cases for the temperature, moisture and stress changes over time. The two finite elements were analysed: one in the interior of the wall, and the second at the surface – both in the mid-span cross-section of the wall. The results are collectively presented in Fig. 14–16. The basic case is denoted as “basic” while the temperature cases $T_z = T_p = 15^\circ\text{C}$ as “mod1”, $T_z = 25^\circ\text{C}$ and $T_p = 20^\circ\text{C}$ as “mod2” and $T_z = 25^\circ\text{C}$ and $T_p = 15^\circ\text{C}$ as “mod3”, respectively.

It was observed that the initial temperature of young concrete and ambient temperature had an influence upon the maximum temperature and heat migration rate during hardening process. The highest temperatures were reached when both the initial temperature of the concrete and the external temperature were high, lower when initial cooling of the concrete mix was applied and the lowest when the two were on the same, low level. In all cases, the maximum temperature was reached after almost the same time, but there was an impact on the cooling rate: cooling was finished at the same time, so it proceeded faster in the walls in which concrete was initially warmer. The process was more moderate in the near-surface parts than in the interior of the wall. There was a negligibly small influence of the temperature difference on the moisture dissipation process. Two general characteristics were observed: the first, smooth, characterising internal parts and the second, with a visible drop, in the surface parts.

In the stress–time relationship, the difference between the internal and surface areas was also noticed: compressive stresses were lower near the surface but the peak tensile stress was observed earlier. Lowering of the initial concrete temperature allowed more moderate stress change of the smaller magnitude in tension to be obtained, especially if achieved by initial cooling of concrete. Pre-cooling of concrete mix allowed for the elimination of cracking. Concreting at a lower temperature allowed for the lowering of the values of stresses, but at the same time a lower temperature resulted in a slower rate of strength development. This explains a similar level of damage intensity of the wall executed in $T_z = T_p = 15^\circ\text{C}$ conditions.

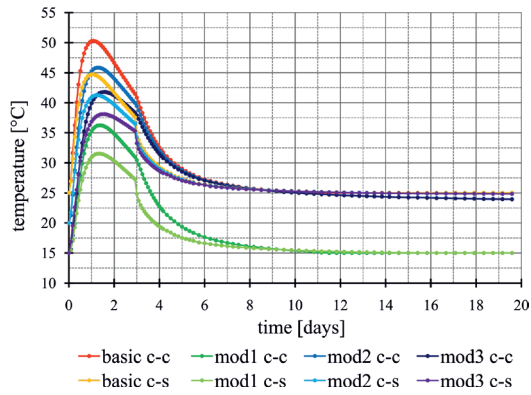


Fig. 14. Temperature development over time – influence of concreting conditions

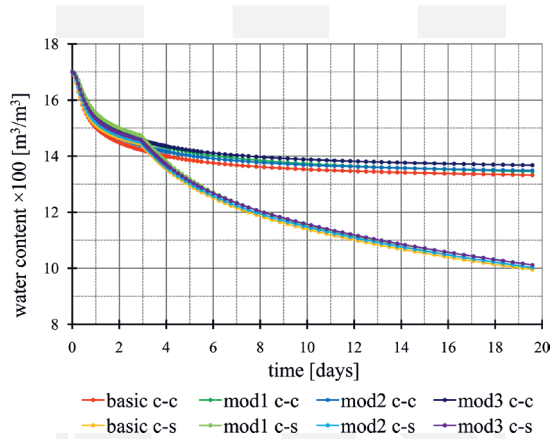


Fig. 15. Moisture loss over time – influence of concreting conditions

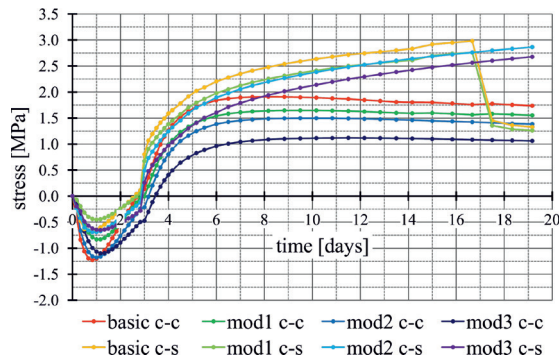


Fig. 16. Stress development over time – influence of concreting conditions

4.4.2. Influence of time of formwork removal

Formwork removal after 3 days was assumed in the basic case. However, it was proved that at this moment, young concrete has still very high temperature and is subjected to high thermal strains. Therefore, it was investigated how the later formwork removal would influence the cracking of the wall.

The first scenario was analysed in which the formwork was removed after 10 days. The results presented in Fig. 17 show that this is not beneficial for the wall. The level of damage intensity was comparable to the basic case. Another scenario assumed that the wall was in the formwork during the whole process of curing. The removal was assumed after 28 days, so when the concrete had definitely cooled down. The maps in Fig. 18 show that significant limitation of cracking was obtained. What is important is that the application of the formwork during the whole curing process prevented the surface of the wall from rapidly drying and heat dissipation was limited. Hence, higher stresses occurred in the interior of the wall.

A collective comparison was made to assess the influence of different times of the formwork removal. The results are presented in Fig. 19 for temperatures, Fig. 20 for moisture and Fig. 21 for stresses. The case when formwork was removed after 10 days was denoted as “mod4” and when the wall was detained in formwork for 28 days as “mod5”.

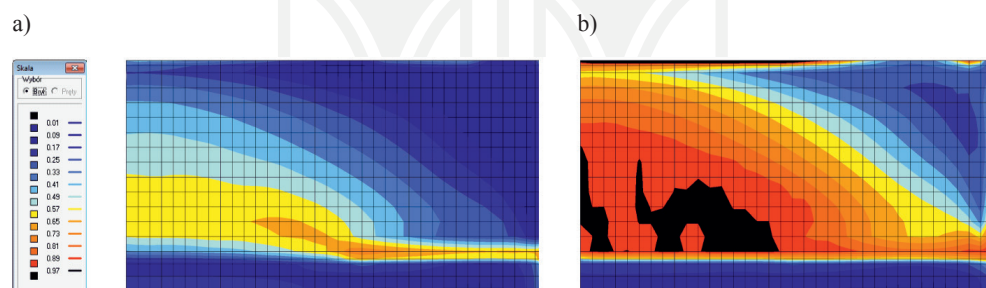


Fig. 17. Damage intensity of the wall in 19 days (formwork removed after 10 days): a) $XZ = 0$, b) $XZ = 0.4$ m

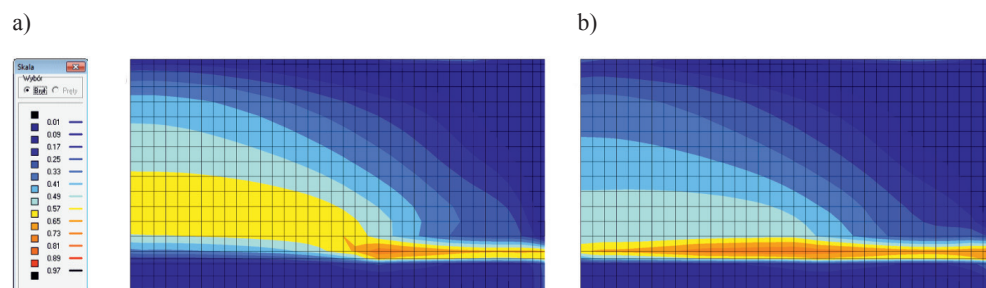


Fig. 18. Damage intensity of the wall in 19 days (the wall detained in formwork): a) $XZ = 0$, b) $XZ = 0.4$ m

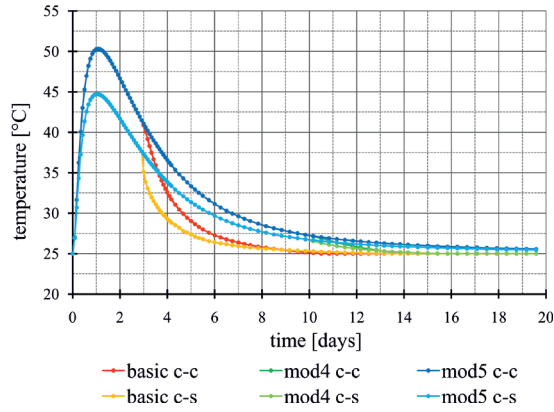


Fig. 19. Temperature development over time – influence of formwork removal time

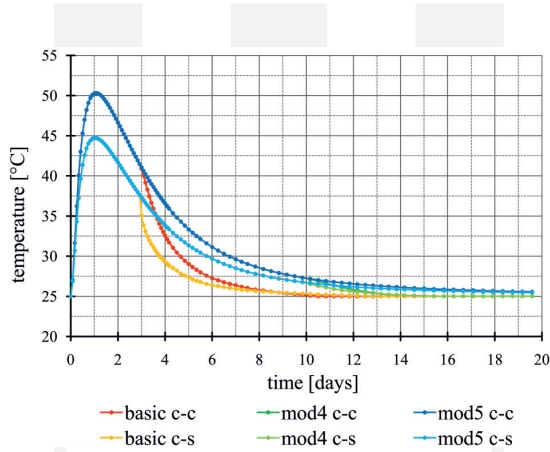


Fig. 20. Moisture loss over time – influence of formwork removal time

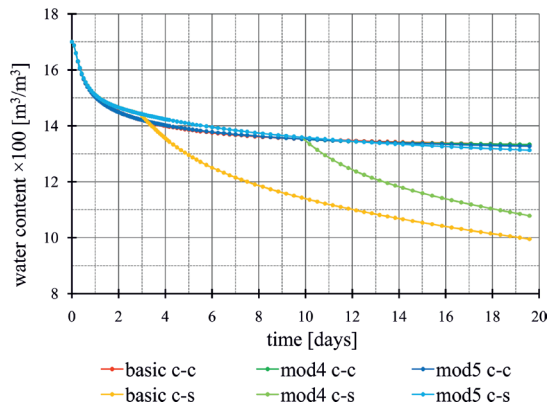


Fig. 21. Stress development over time – influence of formwork removal time

The time of the formwork removal had an influence on the rate of cooling and moisture migration after the removal. The most significant effects were observed when the formwork was removed early and the process attenuated when the formwork was detained for a longer time. A uniform temperature change was observed when the formwork was not removed until the concrete had cooled down.

The rate and magnitude of the water removal was almost the same both for the internal and surface parts unless the formwork was removed, this triggered extensive dehydration of the near-surface areas.

The stress development was identical when the wall was in the formwork. After the formwork removal, when the concrete of the wall started to shrink, the value of the peak tensile stress was greater and occurred earlier in the walls where the formwork was removed early; this led to surface cracking. What was very interesting, for the wall which was detained in the formwork for the whole curing process, was that the tensile stress curve was very smooth and the greatest stresses were observed in the interior of the wall. This had the result of no possibility of exchange of heat and moisture with the surrounding.

5. Conclusions

The presented paper deals with the numerical modelling of thermal–moisture effects in hardening concrete on the example of a reinforced concrete wall cast against an old set foundation. The results obtained in the numerical analyses conform to the present knowledge and practical experience. Because of a complex nature of a multi-phenomena process of concrete hardening numerical analyses are particularly difficult. The results can be regarded as qualitatively and quantitatively correct because the model was validated with experimental data. This confirms that the proposed numerical model of thermal–moisture effects in young concrete describes correctly the analysed case. In conclusion, the contribution of the presented work to this field of activity is the development and adaptation of a complex numerical model of thermal–moisture effects in hardening concrete and its implementation.

This paper was done as part of a research project N N506 043440 funded by Polish National Science Centre.

References

- [1] Ayotte E., Massicotte B., Houde J., Gocovski V., *Modeling the thermal stresses at early ages in a concrete monolith*, ACI Materials Journal, vol. 94 issue 6, 1997.
- [2] Bažant Z. P., Carol I., *Viscoelasticity with aging caused by solidification of nonaging constituent*, Journal of Engineering Mechanics, no. 119, 1993.
- [3] Borucka-Lipska J., Kiernożycki W., Freidenberg P., *Indirect interactions in massive concrete elements with different concrete compositions*, Przegląd Budowlany, nr 3, 2006.
- [4] Di Luzio G., Cedolin L., *Numerical model for time-dependent fracturing of concrete structures and its application*, Proceedings of International Conference on Fracture Mechanics of Concrete and Concrete Structures, Catania, Italy 2007.

- [5] Santurjian O., Kolarow L., *A spatial FEM model of thermal stress state of concrete blocks with creep consideration*, Computers and Structures, vol. 58 issue 3, 1996.
- [6] Yuan Y., Wan Z.L., *Prediction of cracking within early-age concrete due to thermal, drying and creep behavior*, Cement and Concrete Research, no. 32, 2002.
- [7] Gawin D., Pesavento F., Schrefler B. A., *Hygro-thermo-chemo-mechanical modelling of concrete at early ages and beyond. Part I: Hydration and hygro-thermal phenomena*, International Journal for Numerical Methods in Engineering, no. 67, 2006.
- [8] Gawin D., Pesavento F., Schrefler B.A., *Hygro-thermo-chemo-mechanical modelling of concrete at early ages and beyond. Part II: Shrinkage and creep of concrete*, International Journal for Numerical Methods in Engineering, no. 67, 2006.
- [9] Wyrzykowski M., *Modeling coupled thermo-hygral process in maturing concrete exposed to internal and external curing*, PhD thesis, Technical University of Łódź, Łódź 2010.
- [10] Andreasik M., *Thermal-shrinkage stresses in massive concrete*, PhD thesis, Cracow Technical University, Kraków 1982.
- [11] Szarliński J., *Stress state and limit loads of massive concrete structures*, Monograph 88, Kraków 1989.
- [12] Klemczak B., *Viscoelastic-plastic material model for numerical simulation of phenomena occurring in early age concrete*, PhD thesis, Silesian University of Technology, Gliwice 1999.
- [13] Meschke G., *Consideration of aging of shotcrete in the context of 3-D viscoplastic material model*, International Journal for Numerical Methods in Engineering no. 39, 1996.
- [14] Tanabe T., Ishikawa Y., Ando N., *Visco-elastic and visco-plastic modeling of transient concrete*, Proceedings of EURO-C 1998 International Conference on Computational Modelling of Concrete Structures, Badgastein, Austria 1998.
- [15] Klemczak B., *Modeling thermal-moisture and mechanical effects in massive concrete structures*, Monograph 183, Silesian University of Technology, Gliwice 2008.
- [16] Klemczak B., *Prediction of Coupled Heat and Moisture Transfer in Early-Age Massive Concrete Structures*, Numerical Heat Transfer. Part A: Applications, vol. 60, no. 3, 2011.
- [17] *CEB-FIP Model Code 1990*, 1991.
- [18] Klemczak B. *Adapting of the Willam-Warnke failure criteria for young concrete*, Archives of Civil Engineering, vol. 53, no. 2, 2007.